Gas Separation by Pressure Swing Adsorption: A Pore-Diffusion Model for Bulk Separation

An experimental and theoretical study is performed for bulk separation of gas mixture by pressure swing adsorption, a process widely used commercially for gas purification. By cycling the pressure of a bed of activated carbon between 3 and up to 500 psig (0.021 to 3.445 MPa), at the ambient temperature, a 50/50 H_2/CH_4 mixture is separated into two products with well over 90% purity and recovery at high throughputs. All process characteristics can be predicted by a pore-diffusion model. A fundamental understanding of the function of each step in the cyclic process is given.

R. T. YANG and S. J. DOONG

Department of Chemical Engineering
State University of New York at Buffalo
Buffalo, NY 14260

SCOPE

An increasing number of commercial applications have been recently found for pressure swing adsorption (PSA) because of its low energy requirements and costs. However, the applications have been somewhat limited to purification processes in which the less-adsorbed component is the desired product. Bulk separation, where all components are wanted products, is still in its infancy. The theoretical understanding of PSA is, as revealed in the open literature, also primitive. The published models for PSA and related cyclic separation processes are predominantly based on the equilibrium assumption for the fluid/solid system. Most of them considered the adsorption of a single, dilute adsorbate (Pigford et al., 1969; Sweed and Wilhelm, 1969; Wankat, 1981; Hill et al. 1981, 1982, 1983). Kadlec et al. (1971, 1972) modeled a single-column process similar to PSA for separating 28.4% N_2 in CH_4. In this work, bulk separation is studied both experimentally and theoretically for a mixture of 50/50 H_2/CH_4. The results are analyzed for both components in terms of product purity, product recovery, and sorbent productivity. The theoretical model embodies all important elements in bulk separation: pore-diffusion resistance, nonisothermality, and adsorption of all components (by using a noniterative model for adsorption of mixtures).

CONCLUSIONS AND SIGNIFICANCE

Separation of a 50/50 H_2/CH_4 mixture by activated carbon is accomplished by PSA involving five cyclic steps:

(I) pressurization
(II) adsorption
(III) cocurrent depressurization
(IV) countercurrent blowdown
(V) purge

The less strongly adsorbed component, H_2, is produced by steps II and III, and CH_4 is produced by steps IV and V. (Continuous feed and products are made possible by using a battery of interconnected beds.)

Both products are produced at well over 90% purity and recovery, at high feed throughputs. The pore-diffusion model successfully predicts all process characteristics and provides insights into the principles underlying each step of the cycle. The computation involved in the model is light (at 1 min/cycle in a Cyber 730 computer) because of simplifying assumptions used. The product purity of the strongly adsorbed component depends critically on the use of step III. The main function of this step is to elute the less strongly adsorbed component out of the concentration wavefront, which increases the loading of the strongly adsorbed component into the bed. The purge step by the less strongly adsorbed component is crucially important in the product purity of the same component. Repressurization by this component, instead of the feed mixture, also enhances its product purity.

INTRODUCTION

Pressure swing adsorption (PSA) is a gas separation process in which the adsorbent is regenerated by reducing the partial pressure of the adsorbed component. Partial pressure reduction can be accomplished rather rapidly by lowering the total pressure or using a purge gas. The process was invented by Skarstrom (1959) who suggested that two steps, adsorption and depressuriza-

15475905, 1985, 11, Downloaded from https://aiche.onlinelibrary.wiley.com/doi/10.1002/aic.690311109 by Georgia Institute Of Technology, Wiley Online Library on [06/11/2022]. See the Terms and Conditions (https://onlinelibrary.wiley.com/terms-and-conditions) on Wiley Online Library for rules of use; OA articles are governed by the applicable Creative Commons License

tion/purge, be carried out in two adsorbent beds operated in tandem, thus enabling the processing of a continuous feed. The rapid pressure changes result in short cycles and hence high throughputs, but also make the dynamics of the gas-solid system more difficult to understand.

Since the introduction of the Skarstrom cycle, many more sophisticated PSA processes have been developed and commercialized. PSA has attracted increasing interest more recently because of its low energy requirements as well as low capital investment costs (Stewart and Heck, 1969). State-of-the-art reviews of the PSA processes may be found in Keller (1983), Cassidy and Holmes (1984), and Wankat (1981). In modern PSA processes, three or more beds are used to synchronize and accommodate two additional steps to those in the Skarstrom cycle: cocurrent depressurization and pressure equalization. The two major applications of PSA have been air drying and hydrogen purification. Other commercial applications are oxygen or nitrogen (but not both in the same process) production from air, octane improvement (using Union Carbide ISOSIV Process), and solvent recovery (Cassidy and Holmes, 1984; Keller, 1983). A variation of PSA, first described by Turnock and Kadlec (1971), and Kowler and Kadlec (1972), involves a one-column process driven by a square feed pressure variation applied to one end of the column, with slow withdrawal of a product stream from the opposite end. A process similar to this but using a different pressure cycle, i.e., a short feed and a long exhaust which result in better separation, has recently been commercialized for medical oxygen purposes (Jones and Keller, 1981).

Despite the increasing industrial use of PSA, theoretical understanding of the process is still in a primitive stage. Brief reviews of the theoretical developments have been made by Cheng and Hill (1983), Wankat (1981), and Chen and Yang (1985). In all of the published PSA models, (1) linear adsorption isotherms are used, thus limiting the models to adsorption of dilute species, and (2) local equilibrium between the bulk gas phase and the intraparticle adsorbed phase is assumed, implying no mass transfer limitations. The only exceptions to (2) are the model by Chihara and Suzuki (1983a), and that by Carter and Wyszynski (1983) where the linear-driving-force approach for mass transfer rates is used. In the study by Kadlec et al. (1971; 1972) on the cyclic process which is related to PSA, a Freundlich isotherm was used for the total amount adsorbed and a constant "relative volatility" factor was used for the two components. The analytical approach of the equilibrium models is similar to earlier models for the processes of parametric pumping (Sweed and Wilhelm, 1969; Jenczewski and Myers, 1968; Pigford et al., 1969; Aris, 1969), including the complexities of the blowdown and pressurization steps. The method of characteristics is used in these models to derive simple algebraic equations in order to estimate the steady-state performance for simplified PSA cycles. The equilibrium models include those of Shendalman and Mitchell (1972), Weaver and Hamrin (1974), Fernandez and Kenney (1983), Hill et al. (1982), for one adsorbate, and the models of Chan et al. (1981) and Nataraj and Wankat (1982), for two or more adsorbates. The other approach involves numerical solution of mass and energy balance equations plus the mass transfer rate equations, and provides better approximations at the expense of increased computation time (Chihara and Suzuki, 1983a; Carter and Wyszynski, 1983). All of the above-mentioned models pertain to dilute systems and thus linear isotherms are used.

Multicomponent, bulk gas separation, i.e., for gases containing high concentrations of adsorbates (more than 10 wt % according to Keller, 1983), is in its infancy from the point of view of both commercial application and theoretical understanding. However, its potential applications are imminent and important. One such application is the separation of fuel gases such as H_2 and CH_4 from coal gasification processes. (The bulk separation of H_2/CH_4 is also important in petroleum and chemical processing industries). In bulk separation using PSA, the temperature variation is large (25–45°C for the H_2/CH_4 system, as will be shown in this paper) when compared to that in purification processes (±3°C in air drying, Chihara and Suzuki, 1983b). Thus, energy balance equations must be included in modeling. Furthermore, linear adsorption isotherms will not be applicable for bulk separation, and a predictive model for adsorption from gas mixtures should be used. This paper describes a model embodying both energy balance and a model for adsorption from gas mixtures, as well as the mass transfer limitation due to pore diffusion in the adsorbent. Employing the model system CH_4/H_2/activated carbon, the pore-diffusion model is successfully used to predict the results of all five basic steps in PSA.

PROCESS DESCRIPTION

In a typical PSA bed process, each bed goes through some or all of the following five basic steps forming a cycle:

(I) pressurization
(II) adsorption
(III) cocurrent blowdown
(IV) countercurrent blowdown
(V) purge

Two or more interconnected beds are operated in phase so continuous feed and products are possible. A two-bed arrangement is shown in Figure 1 for continuous bulk separation of a mixture such as H_2/CH_4.

In step I, bed 1 is pressurized to the feed pressure by the feed (or by the blowdown gases, which are the less adsorbable gases from other beds as practiced in industry). In step II, the high pressure feed flows through bed 1 while a portion of the effluent H_2 product is used to purge bed 2 at a reduced pressure. Step III, cocurrent blowdown, is used to recover the H_2 remained in the voids and to allow time for CH_4 to desorb in the bed. The end pressure of step III depends on bed utilization, i.e., fraction of the bed covered by the CH_4 wavefront. Steps IV and V are both operated countercurrent to the feed direction to produce CH_4 and provide a cleaned bed for the next cycle.

The performance of a PSA process is determined by three interrelated sets of results: product purity, product recovery, and productivity. The productivity is judged as the rate of feed processed per unit amount of sorbent. For bulk separation each product must be considered for product recovery and purity. All these factors will be predicted by the pore-diffusion model.

THE PORE-DIFFUSION MODEL

To simplify the derivation and calculation, the following assumptions and approximations are made:

1. Ideal gas law applies. [The compressibility factor for the gas mixture was calculated to be 0.99 under our experimental condition of 34 atm (101.3 kPa) and 25°C.]
2. The axial pressure gradient across the bed is neglected.
3. Plug-flow condition holds; i.e., axial dispersion is neglected. (This assumption is in fact not necessary, as inclusion of the dispersion term in the model did not show any difference in the results).
4. Thermal equilibrium is assumed between the fluid and the particles.
5. No variation exists in the radial direction for both concentration and temperature.
6. Due to the narrow temperature range of the process, transport (diffusivity) and physical (C_p, ρ) properties are assumed to be independent of temperature.

Mass Balances in Packed Bed and in Pores

Mass balances for both components $CH_4(A)$ and $H_2(B)$ in the

15475905, 1985, 11, Downloaded from https://aiche.onlinelibrary.wiley.com/doi/10.1002/aic.690311109 by Georgia Institute Of Technology, Wiley Online Library on [06/11/2022]. See the Terms and Conditions (https://onlinelibrary.wiley.com/terms-and-conditions) on Wiley Online Library for rules of use; OA articles are governed by the applicable Creative Commons License

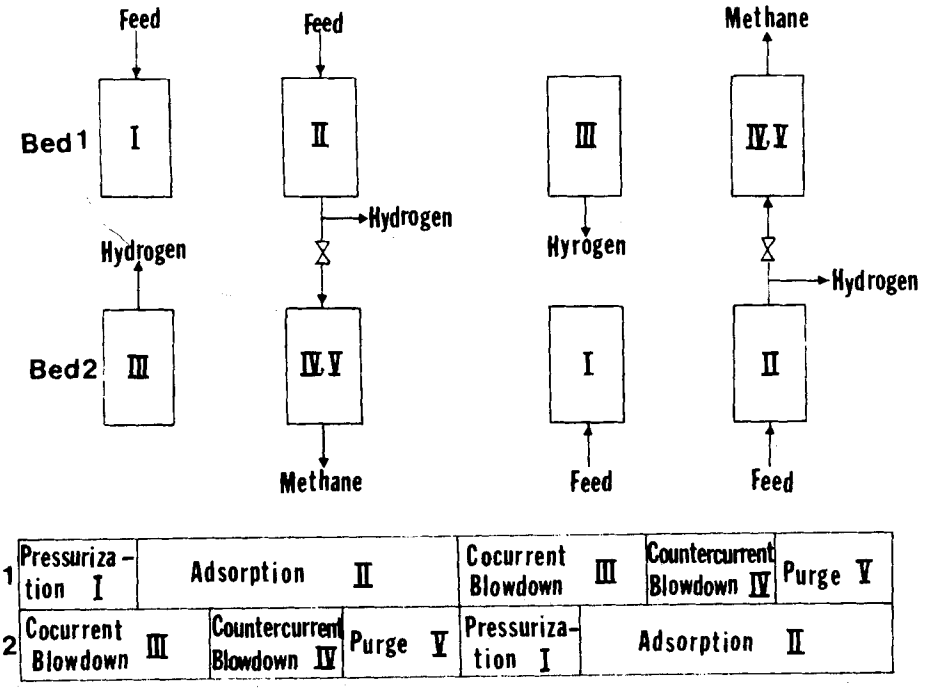

Figure 1. Cycle schematic of steps I–V in a two-bed pressure swing adsorption process.

packed-bed-column at system pressure P and temperature T are given by:

$$\alpha \frac{\partial C_A}{\partial t} + \frac{\partial u C_A}{\partial z} - S_A = 0 \tag{1}$$

and

$$\alpha \frac{\partial C_B}{\partial t} + \frac{\partial u C_B}{\partial z} - S_B = 0 \tag{2}$$

where C_A and C_B are the concentrations of CH_4 and H_2, respectively, in bulk flow, and α is the interparticle void fraction. The velocity u is the superficial velocity, i.e., volumetric flow rate through a unit cross-sectional area of the column. S_A and S_B are the sorption rates per unit volume of bed.

Applying ideal gas law, $C = P/RT$ and $C_A = Py_A/RT$, the following replace Eqs. 1 and 2:

$$\alpha \frac{\partial y_A}{\partial t} + u \frac{\partial y_A}{\partial z} + y_A \frac{RT}{P}(S_A + S_B) - \frac{RT}{P} S_A = 0 \tag{3}$$

$$\alpha \frac{\partial P}{\partial t} - \frac{\alpha P}{T}\frac{\partial T}{\partial t} + P\frac{\partial u}{\partial z} - \frac{uP}{T}\frac{\partial T}{\partial z} - RT(S_A + S_B) = 0 \tag{4}$$

Mass balance for A and B inside the pores of a spherical sorbent particle at a given location (z) yields:

$$\epsilon \frac{\partial C_{AP}}{\partial t} + \frac{1}{r^2}\frac{\partial}{\partial r}(r^2 N_{Ar}) + \rho_p \frac{\partial q_A}{\partial t} = 0 \tag{5}$$

$$\epsilon \frac{\partial C_{BP}}{\partial t} + \frac{1}{r^2}\frac{\partial}{\partial_r}(r^2 N_{Br}) + \rho_p \frac{\partial q_B}{\partial t} = 0 \tag{6}$$

where ϵ is the intraparticle void fraction, subscript P indicates concentrations inside the pores, and the other terms are as listed in the notation.

To simplify the computation, the following particle volume average quantities are defined:

$$\overline{C_{AP}} = \frac{3}{a^3}\int_0^a C_{AP} r^2 dr;\ \overline{y_{AP}} = \frac{3}{a^3}\int_0^a y_{AP} r^2 dr \tag{7}$$

$$\overline{q_A} = \frac{3}{a^3}\int_0^a q_A r^2 dr \tag{8}$$

$$\overline{q_B} = \frac{3}{a^3}\int_0^a q_B r^2 dr \tag{9}$$

Further, the sorption rates may be related to the fluxes at the pore mouths, or at the particle surface:

$$N_A^s = N_{Ar}|_{r=a} = y_{AP}^s(N_A^s + N_B^s) - CD_e \frac{\partial y_{AP}}{dr}|_{r=a} \tag{10}$$

The two terms in Eq. 10 refer to convective and diffusive fluxes, respectively.

By integrating Eqs. 5 and 6 with respect to r and using the particle volume averaged quantities, we have

$$N_A^s + N_B^s = -\frac{a}{3}\frac{\epsilon}{RT}\frac{\partial P}{\partial t} + \frac{a}{3}\frac{\epsilon P}{RT^2}\frac{\partial T}{\partial t} - \frac{a}{3}\rho_P\left(\frac{\partial \bar{q}_A}{\partial t} + \frac{\partial \bar{q}_B}{\partial t}\right) \tag{11}$$

Equation 11 relates the total flux in or out of the pores with the rates of changes of temperature, pressure and adsorption capacities.

To further simplify the model, we assume a parabolic concentration profile within each particle. This is an approximation used previously (Liaw et al., 1979) which is indeed a good one when compared with the computed profiles (Tsai et al., 1983). Thus, we have

$$y_{AP} = A_0 + A_2 r^2$$

$$A_0 = y_{AP}^s - A_2 a^2$$

$$A_2 = (y_{AP}^s - \bar{y}_{AP})\frac{5}{2a^2} \tag{12}$$

15475905, 1985, 11, Downloaded from https://aiche.onlinelibrary.wiley.com/doi/10.1002/aic.690311109 by Georgia Institute Of Technology, Wiley Online Library on [06/11/2022]. See the Terms and Conditions (https://onlinelibrary.wiley.com/terms-and-conditions) on Wiley Online Library for rules of use; OA articles are governed by the applicable Creative Commons License

or,

$$\frac{\partial y_{AP}}{\partial r}\Big|_{r=a} = (y^s_{AP} - \bar{y}_{AP})\frac{5}{a} \tag{13}$$

Combining Eqs. 5, 10, 11 and 13, the following is obtained:

$$\frac{\partial \bar{y}_{AP}}{\partial t} = (y^s_{AP} - \bar{y}_{AP})\frac{1}{P}\frac{\partial P}{\partial t} - (y^s_{AP} - \bar{y}_{AP})\frac{1}{T}\frac{\partial T}{\partial t} + (y^s_{AP} - \bar{y}_{AP})\frac{15D_e}{a^2\epsilon} - \frac{\rho_p RT}{\epsilon P}\frac{\partial \bar{q}_A}{\partial t} + \frac{\rho_p RT}{\epsilon P}y^s_{AP}\left(\frac{\partial \bar{q}_A}{\partial t} + \frac{\partial \bar{q}_B}{\partial t}\right) \tag{14}$$

Equilibrium Adsorption from Gas Mixture

Several models exist in the literature for predicting adsorption of each component in a gas mixture from single gas isotherms (Chen and Yang, 1985). The only noniterative method, however, is the loading ratio correlation (LRC). The LRC equations can be derived from the Langmuirian kinetic approach. Although its theoretical basis is not as rigorous as other models using the thermodynamic approach, it fits experimental data equally as well, as shown for zeolites (Yon and Turnock, 1971) and activated carbon, which will be used in this work (Chen and Yang, 1985).

The LRC equations for the binary mixture are:

$$q_A = \frac{q_{mA} B_A p^a y^a_{AP}}{1 + B_A p^a y^a_{AP} + B_B p^b (1 - y_{AP})^b} \tag{15}$$

$$q_B = \frac{q_{mB} B_B p^b (1 - y_{AP})^b}{1 + B_A p^a y^a_{AP} + B_B p^b (1 - y_{AP})^b} \tag{16}$$

The equilibrium constants B_A and B_B are functions of temperature. q_A, q_B and y_{AP} can all be expressed as particle volume averaged quantities, and a and b are constants.

The time derivatives are

$$\frac{\partial \bar{q}_A}{\partial t} = \frac{\partial \bar{q}_A}{\partial P}\frac{\partial P}{\partial t} + \frac{\partial \bar{q}_A}{\partial T}\frac{\partial T}{\partial t} + \frac{\partial \bar{q}_A}{\partial \bar{y}_{AP}}\frac{\partial \bar{y}_{AP}}{\partial t} \tag{17a}$$

and

$$\frac{\partial \bar{q}_B}{\partial t} = \frac{\partial \bar{q}_B}{\partial P}\frac{\partial P}{\partial t} + \frac{\partial \bar{q}_B}{\partial T}\frac{\partial T}{\partial t} + \frac{\partial \bar{q}_B}{\partial \bar{y}_{AP}}\frac{\partial \bar{y}_{AP}}{\partial t} \tag{17b}$$

A working equation for $\partial \bar{y}_{AP}/\partial t$ can be obtained by substituting Eqs. 17a and 17b into Eq. 14. The derivatives of $\bar{q}_A$ and $\bar{q}_B$ with respect to P, T, and $\bar{y}_{AP}$ can be obtained from Eqs. 15 and 16. (The temperature dependence of the equilibrium constants will be given below).

The local rates of adsorption, S_A and S_B, are calculated from $\bar{y}_{AP}$:

$$S_A = \frac{3\rho_B}{\rho_p}\frac{1}{a}[N_{Ar}]_{r=a} \tag{18a}$$

$$S_B = \frac{3\rho_B}{\rho_p}\frac{1}{a}[N_{Br}]_{r=a} \tag{18b}$$

where the flux N_r is calculated using Eqs. 10, 11 and 13.

Energy Balance in the Bed

Energy balance in the bed gives:

$$(\alpha'\rho_g C_{pg} + \rho_b C_{ps})\frac{\partial T}{\partial t} + \rho_g C_{pg} u\frac{\partial T}{\partial z} - Q_A\rho_b\frac{\partial \bar{q}_A}{\partial t} - Q_B\rho_b\frac{\partial \bar{q}_B}{\partial t} + \frac{2h}{R}(T - T_w) = 0 \tag{19}$$

where α' is the total void fraction and $\alpha' = \alpha + \epsilon(1 - \alpha)$. The last term is necessary since the diameter of the bed in the experimental unit is small and the wall (stainless steel) is thick. The heat capacity of the wall also cannot be neglected except for a commercial PSA unit. The temperature of the wall is given by:

$$\rho_w C_{pw} A_w\frac{\partial T_w}{\partial t} = 2\pi Rh(T - T_w) \tag{20}$$

Boundary Conditions

$$y_A(t,z = 0) = y_{in}, \quad T(t,z = 0) = T_{in} \quad \text{(Steps I, II)} \tag{21}$$

$$y_A(t,z = L) = 0, \quad T(t,z = L) = T_{in} \quad \text{(Step V)} \tag{22}$$

$$u(t,z = L) = 0 \quad \text{(Steps I, IV)} \tag{23}$$

$$u(t,z = L) = u_{out} \quad \text{(Step II)} \tag{24}$$

$$u(t,z = 0) = 0 \quad \text{(Step III)} \tag{25}$$

$$u(t,z = L) = u_p \quad \text{(Step V)} \tag{26}$$

$$P = P(t) \quad \text{(All Steps)} \tag{27a}$$

or, $u(t,z = 0) = u(t)$ (Step I); $u(t,z = L) = u(t)$ (Steps III and IV);

$$P = P_{feed} \text{ (Step II)}; \quad P = P_{purge} \quad \text{(Step V)} \tag{27b}$$

Either Eq. 27a or 27b can be used as the boundary condition. $P(t)$, as recorded by the pressure transducer, is used in this work, and $u(t)$ is calculated. Alternatively, Eq. 27b can be used and $P(t)$ and other results can be calculated. In this case, the product flowrate in III and IV, the feed rate in I, and the high and low pressure are used, which is similar to the approach of Kadlec et al. (1971, 1972). The value of T_{in} is 293 K, and u_{out} and u_p are measured quantities.

NUMERICAL SOLUTION OF THE MODEL AND REQUIRED INFORMATION

Besides the physical properties of the gas-solid system, additional information is needed for the model: equilibrium adsorption isotherms and pore diffusivity.

Single gas isotherms for the specific system under this investigation (H_2 and CH_4 on PCB activated carbon) have been measured by Saunders (1982), covering the temperature range 295–480 K and pressures up to 1,000 psig (6.99 MPa). The data were best fitted by a hybrid Langmuir-Freundlich isotherm:

$$q_i = \frac{q_{mi} B_i P_i^{ni}}{1 + B_i P_i^{ni}} \tag{28}$$

where for CH_4(A): $q_{mA} = 1.795(1/T)$ gmol/g
$B_A = 3.8 \times 10^{-5} \exp(1.73 \times 10^2/T)$ (1/psi) or (1,489/kPa)
$n_A = a = 1$

and for H_2(B): $q_{mB} = 0.308T^{-0.59}$ (gmol/g)
$B_B = 4.23 \times 10^{-6} \exp(1.23 \times 10^3/T)$ $(1/\text{psi})^{1/n}$
$n_B = b = 0.96$

These data are to be used in the LRC equations, Eqs. 15 and 16. The experimental data on adsorption from H_2/CH_4 mixtures on

15475905, 1985, 11, Downloaded from https://aiche.onlinelibrary.wiley.com/doi/10.1002/aic.690311109 by Georgia Institute Of Technology, Wiley Online Library on [06/11/2022]. See the Terms and Conditions (https://onlinelibrary.wiley.com/terms-and-conditions) on Wiley Online Library for rules of use; OA articles are governed by the applicable Creative Commons License

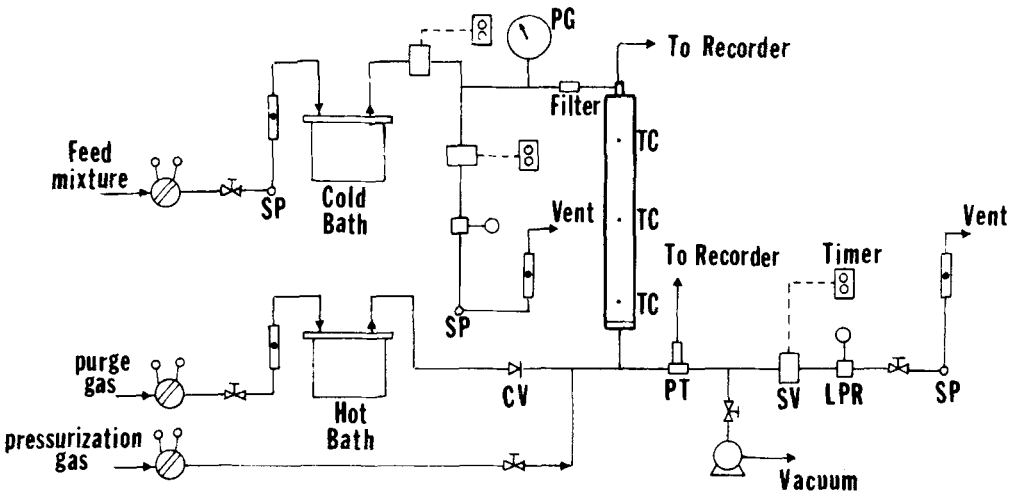

Figure 2. Schematic diagram of apparatus for pressure swing adsorption for gas separation. *SP*, sampling port; *PG*, pressure gauge; *CV*, check valve; *PT*, pressure transducer; *SV*, solenoid valve; *TC*, thermocouple; *LPR*, line pressure regulator.

activated carbon in the wide ranges mentioned above (Saunders, 1982) were fitted with the LRC equations to within 12%, with the exception of one data point for H_2 adsorption at a low H_2 partial pressure, where 20% deviation was obtained (Chen and Yang, 1985).

Isosteric heats of adsorption have also been calculated from the experimental isotherms (Saunders, 1982). The heats of adsorption are rather constant over coverage at 5.00 kcal/mol (20.93 kJ/mol) for CH_4 and 2.88 kcal/mol (12.06 kJ/mol) for H_2.

The calculation of pore diffusivity is indeed complex because the effective diffusivity is dependent upon pressure, temperature, and local flux ratio. The operation ranges for the PSA process considered here are approximately 1–21 atm (0.1–2.13 MPa) for pressure, whereas the temperature varies within ±25° from 20°C. The pores for PCB activated carbon are monodisperse with an average diameter of 16 Å (1.6 nm). Therefore, diffusion is primarily between Knudsen and molecular, or in the transition regime with diffusivity (for A):

$$\frac{1}{D_t} = \frac{1 - 1(+ N_B/N_A)y}{D_m} + \frac{1}{D_k} \tag{29}$$

where the flux ratio N_B/N_A approaches -1.

The effective diffusivity varies with T, P, and local concentration, as well as flux ratio, and D_e is a function of both time and location (z and r). It is then desirable to use a constant value in the model. (However, the variation of D_e is within one order of magnitude in normal PSA operations.) This constant D_e may be evaluated at an average operating condition, e.g., at the mean temperature and pressure. (This approximation is a good one, as will be shown later, because the results of the model are not significantly changed when the value of D_e is varied within the same order of magnitude). At the mean temperature and pressure, $D_t = 3.2 \times 10^{-3}$ cm^2/s for CH_4. The effective diffusivity may be evaluated as:

$$D_e = \frac{\epsilon D_t}{\tau} \tag{30}$$

The porosity (ϵ) is 0.61. The value of the tortuosity (t) for carbon is usually higher than that for catalysts, and $\tau = 10$ is a reasonable estimate for activated carbon (Yang and Liu, 1982). Thus,

$$D_e = 2 \times 10^{-4} \text{cm}^2/s$$

will be used in the model.

In addition to the above parameter, the value of the wall heat transfer coefficient, h, may be evaluated as 3×10^{-3} cal/cm^2/°C/s by using the correlation of Yagi and Wakao (1959).

With the input information on equilibrium adsorption and transport properties, the model can be numerically solved. The working equations are Eqs. 3, 4, 14, 15, 16, 18, 19 and 20. Equations 14 and 20 are first solved for $\bar{y}_{AP}$ and T_w at the next time step using Euler's method with forward difference. (Equation 14 may be written out in an expanded form by substituting Eqs. 15, 16 and 17 into this equation). The values of S_A and S_B are then calculated by using Eq. 18 and the values of $\partial \bar{q}_A/\partial t$ and $\partial \bar{q}_B/\partial t$ obtained from Eqs. 15–17. With the values of S_A and S_B, the superficial velocity, u, is calculated from Eq. 4 at all locations in the bed. Here $\partial T/\partial t$ is evaluated at the last time step, as the influence of $\partial T/\partial t$ on u is smaller than that by $\partial P/\partial t$ and $S_A + S_B$. Finally, with the values of S_A, S_B, $\partial \bar{q}_A/\partial t$, $\partial \bar{q}_B/\partial t$ and u, Eqs. 3 and 19 are solved separately by using the Crank-Nicolson method for y_A and T. The numerical results provide all information needed for evaluating the separation process, such as product purity, product recovery, and throughput (sorbent productivity). The computation has been carried out by using 20 grids in the distance direction of the bed and time intervals as small as 0.2 s (or 1/2,100 of the cycle time). The computation time using a Cyber 730 computer is approximately 1 min for each PSA cycle under the conditions described below (and about 10 cycles are adequate to reach steady state).

EXPERIMENTAL

The experimental apparatus was designed for simulating all five basic steps in the PSA process, and capable of wide-range conditions (high pressure, temperature, flowrate, adiabatic, isothermal, etc.) for multicomponent bulk separation. The apparatus was automated and controlled, with the only manual operations being the collection and analysis of samples, plus the recording of flowrates.

Apparatus for PSA

A schematic diagram of the apparatus is shown in Figure 2. The adsorption column was a stainless steel (type 304) pipe 60 cm long and 4.1 cm I.D. The bottom plate of the column was a stainless steel sintered plate glazed to the column. The column was packed with 20–60 mesh activated carbon (designated PCB, manufactured by Calgon Corporation). Glass

15475905, 1985, 11, Downloaded from https://aiche.onlinelibrary.wiley.com/doi/10.1002/aic.690311109 by Georgia Institute Of Technology, Wiley Online Library on [06/11/2022]. See the Terms and Conditions (https://onlinelibrary.wiley.com/terms-and-conditions) on Wiley Online Library for rules of use; OA articles are governed by the applicable Creative Commons License

TABLE 1. ADSORPTION BED CHARACTERISTICS

Bed Inside Radius, R = 2.05 cm
Bed Length, L = 60 cm.
Particle Size, a = 0.028 cm
Bulk Density, ρ_B = 0.498 g/cm^3
Particle Density, ρ_P = 0.85 g/cm^3
Interparticle Void Fraction, α = 0.43
Intraparticle Void Fraction, ϵ = 0.61
Total Void Fraction = 0.78
Heat Capacity of Carbon, C_{Ps} = 0.25 cal/g/°C
Heat Capacity of Wall, C_{Pw} = 0.11 cal/g/°C
Avg. C_P of Gas Mixture, C_{Pg} = 7.647 cal/gmol/°C

wool was compressed on top of the bed to prevent the carryover of particles. An additional in-line filter (60 μm holes) was installed to keep fine particles from entering the gas lines. All lines were quarter-inch (6.4 mm) stainless steel. Three solenoid valves located at the feed, while cocurrent and countercurrent end points were used to alternately direct the flow into and out of the column. These solenoid valves were activated by electronic timers, which were preset to operate at desired time cycles. A check valve in the purge line prevented any back flow. A pressure transducer outside the bottom of the column was connected to a recorder and provided the pressure history of the process. In addition to the transducer, a pressure gauge connected at the top of the column provided an easy pressure reading.

A layer of insulation covering the column helped make the temperature gradient in the radial direction as small as possible. The insulation also simulated adiabatic operation, which approximates commercial PSA processes when large-diameter beds are used. The axial temperature distribution was measured and recorded at three locations in the bed (nominally top, middle, and bottom). This was done by three fine thermocouples sheathed in a one-eighth-inch (3.2 mm) stainless steel protection tube which was inserted in the center of the packed column.

Gas samples were taken by syringes from two sampling ports which were fitted with septa. The syringes were equipped with locks so samples could be collected in short time intervals (ca. 20–50 s) and stored for later gas chromatography analysis.

Experimental Procedure

The procedure described below was for bulk separation of a H_2/CH_4 (50/50 volume) mixture. The bed was cleaned before each run by degassing with a mechanical pump. Step I, pressurization, was initiated by opening the solenoid valve connected to H_2. The desired column pressure was controlled by the pressure regulator connected to the gas cylinder. Step II, high-pressure adsorption, started when the bottom solenoid valve was opened by the timer. The flowrate in step II was controlled by adjusting a needle valve in the line. Step III, cocurrent depressurization, was effected by closing the feed valve. Step IV, countercurrent blowdown, was achieved by simultaneously closing the bottom valve and opening the valve in the top exhaust line. When the column pressure dropped to 3 psig (0.021 MPa), the check valve opened and started the hydrogen purge, step V.

A 7 min cycle was used in all experiments, with the following time distribution: 0.5 min (step I); 3 min (II); 1.5 min (III); 2 min (IV and V). The highest pressure in the runs was 500 psig (3.445 MPa). The feed rate was in the range of approximately 2–14 L STP/min for use in the small column, and was in the range of commercial operations for PSA gas separation. A cyclic steady state was generally reached after 10 cycles.

RESULTS AND DISCUSSION

This research dealt with bulk separation [separation of gases containing over 10% by weight of adsorbate according to Keller's (1983) definition] where strongly- and weakly-adsorbed components were both wanted products. Fifteen experiments were performed to separate a feed mixture of 50/50 (by volume) H_2 and CH_4 into two high-concentration products. The pore-diffusion model was used to simulate all fifteen runs. The model was indeed capable of predicting all process characteristics and the effects of all operating variables.

TABLE 2. STEADY-STATE RESULTS OF RUN A FOR PSA SEPARATION OF A 50/50 MIXTURE OF CH_4 (A)/H_2(B) (PRESSURE HISTORY AS SHOWN FOR RUN I, FIG. 7)

		Experimental		Theoretical	
Step	Time s	Conc. CH_4	Flow L/min	Conc. CH_4	Flow L/min
II	25	0.6	3.0	0.9	3.0
	70	0.9	3.0	1.1	3.0
	115	1.3	3.0	1.5	3.0
	160	1.8	2.9	1.8	3.0
III	15	4.3	7.6	3.0	7.9
	45	6.5	7.4	5.3	7.4
	75	18.8	5.9	12.0	7.1
IV & V					
	12	94.8	20.7	89.6	24.4
	36	99.0	9.8	95.5	14.8
	60	99.0	6.9	92.6	4.1
	84	89.2	5.5	86.3	3.3
	108	83.2	4.3	80.7	2.5
II	Avg. H_2 Conc.*	98.9		98.6	
	Total Amt.*	8.9		8.2	
III	Avg. H_2 Conc.	90.8		93.2	
	Total Amt.	10.5		10.4	
IV, V	Avg. CH_4 Conc.	94.6		89.9	
	Total Amt.	18.9		19.1	
Total Feed Amt./Cycle		37.7		36.5	
% H_2 Recovery		94.4		92.6	
% CH_4 Recovery		91.8		94.1	

* All concentrations in mol%; amounts in L-STP.

Bulk vs. Trace Separation

The major difference in the two types of PSA processes is the additional step of cocurrent depressurization (step III in our process) for bulk separation. For trace separation, such as the commercial processes of air drying the adsorbed component (A) is not a desired product. In both types of separation, the bed utilization (percent of bed covered by the concentration wavefront) is not high, and is usually a few percent for air drying and nearly one-half for bulk separation. In the cocurrent depressurization (or blowdown) step, the weakly adsorbed component (B) in the voids beyond the concentration wavefront is drawn out of the bed. In the meantime, time is allowed for the adsorbed A behind the wavefront to desorb and diffuse out of the porous particles. This additional time can be important for the subsequent recovery of A during countercurrent blowdown and purge steps, especially when pore diffusion is slow. Therefore, by using a cocurrent blowdown step, the product purity of A will be high. Otherwise, the B remaining in the voids will be mixed with the A product. The recovery of B from the voids in this step also enhances the product recovery of B. (However, the product purity of B is usually slightly lowered). The magnitude of temperature variation during each PSA cycle is another major difference between the two types of processes. The temperature variation in bulk separation can be an order of magnitude higher. For example, the temperature (at midpoint) in our experiments on bulk separation typically varied between 10 and 50°C (see be-

15475905, 1985, 11, Downloaded from https://aiche.onlinelibrary.wiley.com/doi/10.1002/aic.690311109 by Georgia Institute Of Technology, Wiley Online Library on [06/11/2022]. See the Terms and Conditions (https://onlinelibrary.wiley.com/terms-and-conditions) on Wiley Online Library for rules of use; OA articles are governed by the applicable Creative Commons License

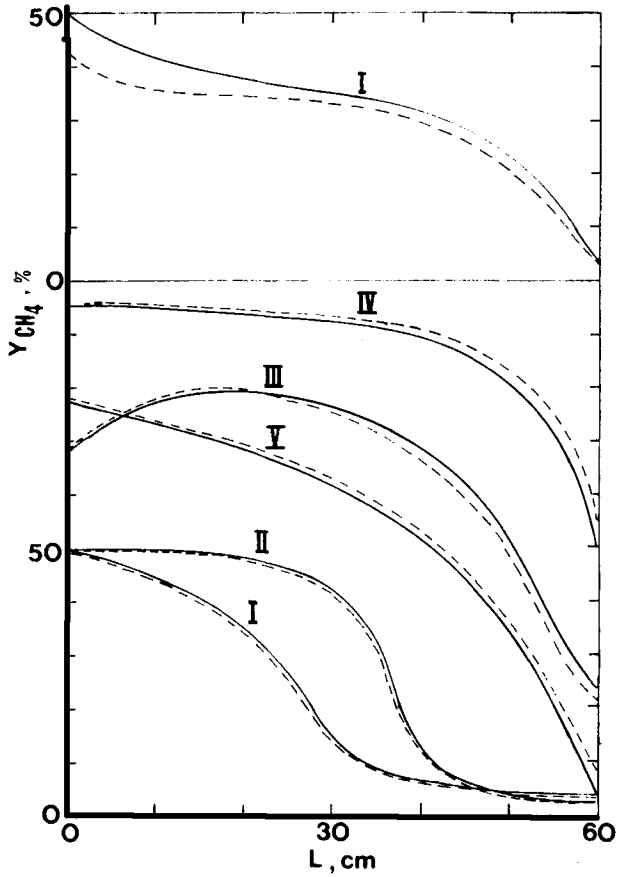

Figure 3. Predicted concentration (in mol%) profile at the end of each step in a steady-state PSA cycle for Run A. The upper figure is at t = 3s in step I. Operating conditions for Run A given in text or Tables 1 and 2. —— mol% in bulk flow; - - - - particle volume averaged concentration ($\bar{y}$). L is distance from feed end.

low), whereas in air drying, the greatest variation was 23 to 29°C (Chihara and Suzuki, 1983b). The large temperature swing has a rather adverse effect on separation. At present, however, no measure has been taken to alleviate this problem.

Presentation of Results of a Typical Run

For all experimental data and model predictions and at steady state, the main results will be presented as concentrations of products, recoveries of products, and sorbent productivity.

The effluents from steps II and III are collected as B product, and those from steps IV and V are A product. The product purity is calculated as the averaged volume concentration over the entire product, and expressed in percent (by vol.). The throughput is presented as the total feed volume (at STP) per cycle. This can be converted into sorbent productivity by dividing the feed rate by the amount of sorbent, 410 g. The product recoveries are defined as:

$$H_2 \text{ Recovery} = \frac{H_2 \text{ from II and III} - H_2 \text{ used in V}}{H_2 \text{ in Feed (in II)}} \quad (31)$$

$$CH_4 \text{ Recovery} = \frac{CH_4 \text{ from IV and V}}{CH_4 \text{ in Feed (in II)}} \quad (32)$$

In Table 1 the characteristics of the packed bed and some physical property data are given. These are applied to all experiments. The experimental results and model prediction values will be first presented for a typical run and designated as run A.

The experimental and model results are compared in Table 2. These are the cyclic steady-state results, which are accomplished approximately after the 10th cycle from startup for all runs. The pressure variation of run A was 300 psig (2.067 MPa) for step II, 70 psig (0.482 MPa) at the end of step III, and 3 psig (0.021 MPa) for step V. (The pressure history was identical to that in run I, depicted in Fig. 7). The experimental results of run A showed that product purity and product recovery of both components well above 90% could be achieved in PSA by using activated carbon. The adsorbent productivity for run A was 0.79 L/hr/g adsorbent, a high value when compared to the commercial PSA process. The model predictions were reasonably good. Note that the pore diffusion model could predict the behavior of all steps in PSA. However, in the previous mass transfer (nonequilibrium) model, the three important steps involving pressure changes (I, III and IV) were assumed "frozen", i.e., no adsorption or desorption was allowed to occur (Chihara and Suzuki, 1983a). As shown in Table 2, all process characteristics for the five steps could be predicted by the model. (Step I is not shown as there was no effluent from this step).

The concentration profiles in bed generated by the model are shown in Figure 3 as bulk flow concentration of methane, y, and volume-averaged pore concentration, $\bar{y}$. The profiles shown here were at the end of each of the five steps at steady state. Since the differences between y and $\bar{y}$ were not large, the operation was probably near "equilibrium." However, the differences between y and $\bar{y}$ could be large during the early period in each step, especially in the steps involving pressure changes. This is illustrated by the concentration profiles at the end of 3 s. in step I, where the differences between y and $\bar{y}$ were not small.

Fourteen other PSA runs and model computations were made to determine the effects on bulk separation by the following variables: purge-to-feed ratio, end pressure of step III (cocurrent blowdown), adsorption pressure, and product flowrate. The effects were also determined of pressurization (step I) with H_2, instead of using the feed mixture. In addition, the results of a hypothetical isothermal PSA run, as predicted by the model, were compared with that of an adiabatic run.

Effect of Purge-to-Feed Ratio

In the original Skarstrom cycle, the times of the high-pressure adsorption step and low-pressure purge are equal. The purge-to-feed ratio is taken as the ratio of linear velocities or flowrates at their respective pressures. In PSA operations, where the two steps have different lengths, such a ratio would not be meaningful. In this situation, as in most commercial multibed processes, a more meaningful expression would be the fraction of gas in the feed that is consumed in the purge step, such as used by Chan et al. (1981). Thus, we define:

$$\text{Purge/Feed Ratio} = \frac{\text{Amt. (L STP) of } H_2 \text{ used in V}}{\text{Amt. (L STP) of } H_2 \text{ inlet in II}} \quad (33)$$

Four experiments (runs B, C, D, E) were conducted to determine the effects of purge-to-feed (P/F) ratio on bulk separation. The overall results are shown in Table 3 and Figure 4. Nearly similar conditions were maintained.

In these, as well as all other experiments, the feed rate (in step II) was controlled by adjusting the product flowrate. This was held nearly constant in all experiments, and the total feed amount per cycle was the sum of all effluents in steps II to V, at cyclic steady-state operation. The calculated total feed amount per cycle for runs B–E, as shown in Table 3 and other tables, included

15475905, 1985, 11, Downloaded from https://aiche.onlinelibrary.wiley.com/doi/10.1002/aic.690311109 by Georgia Institute Of Technology, Wiley Online Library on [06/11/2022]. See the Terms and Conditions (https://onlinelibrary.wiley.com/terms-and-conditions) on Wiley Online Library for rules of use; OA articles are governed by the applicable Creative Commons License

TABLE 3. STEADY-STATE PSA SEPARATION OF 50/50 H_2CH_4 MIXTURE WITH VARIOUS PURGE/FEED RATIOS (PRESSURE HISTORY SHOWN IN FIG. 4)

Run:	Experimental				Theoretical			
	B	C	D	E	B	C	D	E
P/F Ratio	0	0.049	0.066	0.085	0	0.049	0.066	0.085
Step II Avg. % H_2	9.17	93.7	97.4	98.1	89.7	97.4	98.3	99.0
Step II Total Amt.*	12.2	13.2	13.8	14.3	11.0	11.9	12.5	13.1
Step III Avg. % H_2	88.0	88.8	92.6	91.7	86.9	93.6	95.3	96.8
Step III Total Amt.	5.0	6.0	6.1	6.6	5.9	5.6	5.5	5.4
Steps IV, V Avg. % CH_4	80.5	81.5	80.4	81.9	80.6	80.5	80.5	80.4
Steps IV, V Total Amt.	23.1	23.9	25.6	25.4	22.4	24.7	25.5	26.4
Total Feed Amt./Cycle	40.3	42.5	44.6	45.1	39.4	41.6	42.7	43.8
% H_2 Recovery	77.5	79.3	78.3	80.4	76.1	77.7	77.9	77.5
% CH_4 Recovery	92.0	92.6	96.2	96.2	91.8	95.5	96.2	96.8

* All amounts in L STP.

the amount in both step II and step I (pressurization with feed).

The purge step accomplishes two important functions: (1) It strips the adsorbed CH_4 from the bed and hence enriches the CH_4 product purity as well as the CH_4 recovery, and (2) it cleans the bed and prepares the bed for the next cycle, and consequently increases the H_2 product purity. Frequently, the H_2 recovery is increased. These functions of purge are clearly illustrated by the experimental data shown in Table 3 and Figure 4. It is also clear

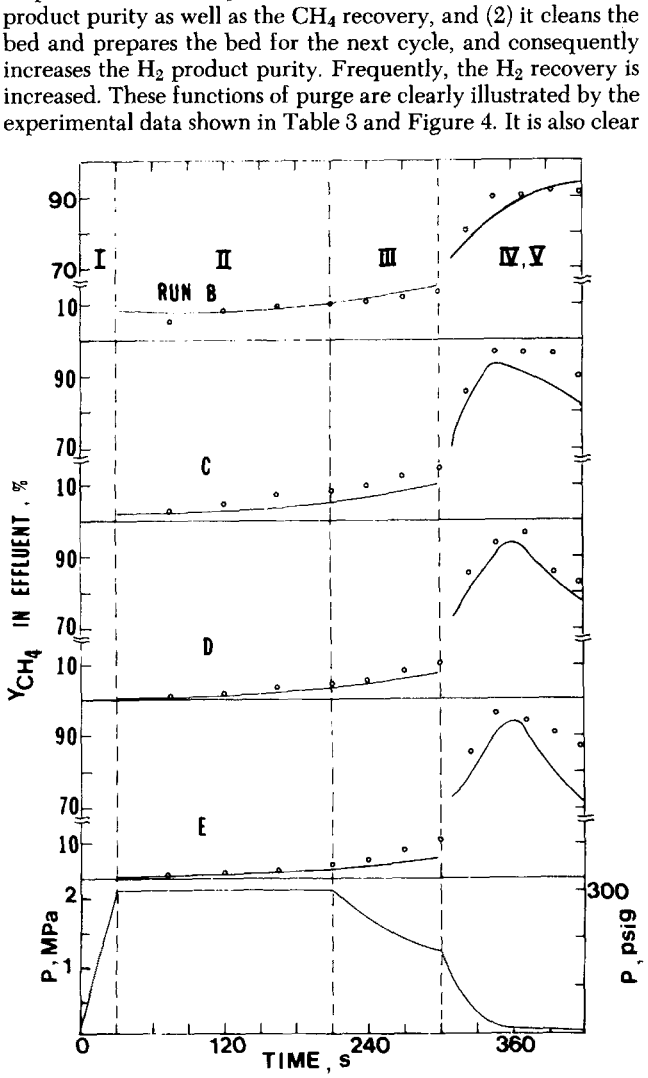

Figure 4. Effluent concentration and pressure input histories in steady-state PSA for Runs B–E; see Table 3 for conditions. O experimental; —— predicted.

that the pore diffusion model is capable of predicting all effects caused by various P/F ratios.

When the P/F ratio is further increased, the H_2 product purity will monotonically increase. However, the following adverse effects will arise: (1) It will dilute the CH_4 product, and (2) will lower the H_2 recovery. It is seen from our results that a P/F ratio in the range of 0.06–0.08 is a likely optimal value. The model is also capable of predicting such an optimal value.

Effects of Cocurrent Depressurization

As mentioned, in bulk separation, cocurrent depressurization is an important step which is often not included in trace separation processes. The cocurrent blowdown step increases hydrogen product recovery as well as CH_4 product purity, for reasons already given. These effects were demonstrated by three experiments (runs F, G, and H) under similar conditions with the exception of the end pressure of cocurrent blowdown. The results are summarized in Table 4. The pressure history and the effluent concentrations are given in Figure 5. As shown by both experimental results and model predictions, the product concentration of CH_4 and the product recovery of H_2 were substantially increased by the cocurrent blowdown step. However, breakthrough (of the CH_4 wavefront) will occur upon excessive cocurrent blowdown, i.e., to an excessively low end pressure. This situation is illustrated by the results of Run H as shown in Figure 5. Consequently, the H_2 product purity and CH_4 recovery both declined when compared with Run G. Thus, the end blowdown pressure of 170 psig (1.17 MPa), as in run G, appeared to be optimal. These important characteristics could all be predicted by the model.

In runs F, G and H, the end pressure of cocurrent blowdown was varied, however the time of blowdown was fixed at 90 s. The rate of blowdown apparently also has strong effects on separation, which has not been investigated in this study (but observed in another study in this laboratory).

The Roles of Bed Voids

In the foregoing, a perhaps overly simplified explanation is given for the functions that are accomplished by the cocurrent depressurization step (step III). A better understanding of this step as well as the effects of pressure and fractional bed utilization in adsorption can be obtained by the following analysis.

The bed voids play a very important, although undesired, role in all steps in PSA. The voids behind (or covered by) the concentration wavefront hold a significant amount of H_2, which limits the CH_4 product purity and H_2 recovery. The total void fraction

Downloaded from https://aiche.onlinelibrary.wiley.com/doi/10.1002/aic.690311107 by Georgia Institute Of Technology, Wiley Online Library on [06/11/2022]. See the Terms and Conditions (https://onlinelibrary.wiley.com/terms-and-conditions) on Wiley Online Library for rules of use; OA articles are governed by the applicable Creative Commons License

TABLE 4. STEADY-STATE PSA SEPARATION OF 50/50 H_2/CH_4 MIXTURE WITH VARIOUS DEGREES OF COCURRENT DEPRESSURIZATION (PRESSURE HISTORIES SHOWN IN FIG. 5)

Run:	Experimental F	Experimental G	Experimental H	Theoretical F	Theoretical G	Theoretical H
End Press. Cocurr. Depressurization, psig	230	170	135	230	170	135
P/F Ratio	0.085	0.090	0.096	0.085	0.090	0.096
Step II Avg. H_2 %	98.5	98.2	98.5	98.9	98.8	98.7
Step II Total Amt.*	8.8	8.7	8.8	7.97	7.93	7.90
Step III Avg. H_2 %	95.5	92.8	84.0	97.0	95.6	93.1
Step III Total Amt.	11.7	14.8	16.0	11.0	13.6	15.4
Steps IV, V Avg. CH_4 %	79.2	89.6	89.5	78.6	84.5	87.8
Steps IV, V Total Amt.	29.7	26.8	24.1	29.6	26.8	25.0
Total Feed/Cycle	49.5	49.6	48.2	47.8	47.7	47.4
% H_2 Recovery	75.6	88.5	89.4	74.6	84.2	89.4
% CH_4 Recovery	97.2	95.1	88.9	97.4	94.9	92.1

* All amounts in L STP.

in the activated carbon bed of this study was 0.78, which was equivalent to 1.612 cm^3 void space per gram of carbon. In the zone covered by the concentration wavefront, the ratio for the amounts of CH_4 to H_2 held in the bed is a strong function of total pressure and gas-phase concentration, as shown in Figure 6. The amount of each component is calculated as the sum of the amounts in the gas phase (using ideal gas law), and in the adsorbed phase (using loading ratio correlation).

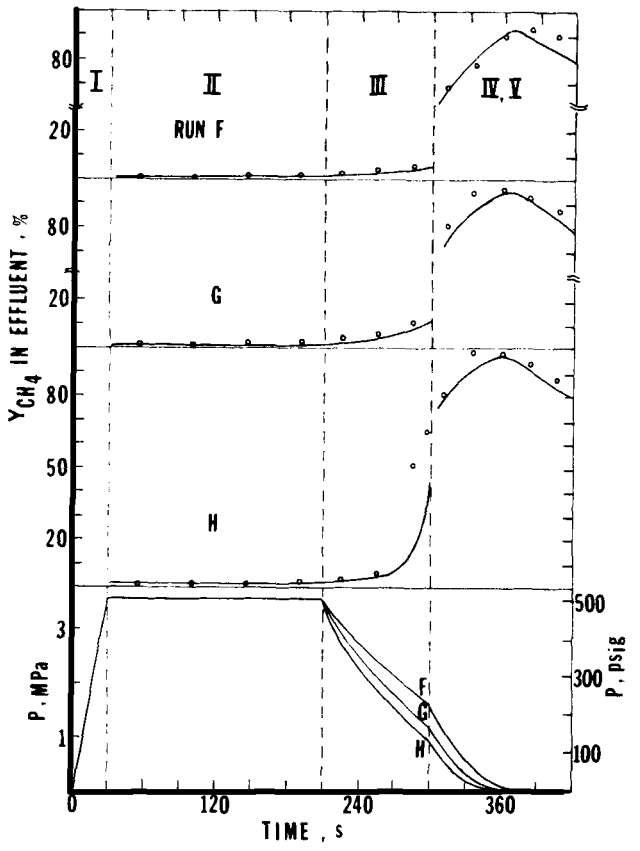

Figure 5. Effluent concentration and pressure input histories in steady-state PSA; see Table 4 for conditions. O experimental; —— predicted.

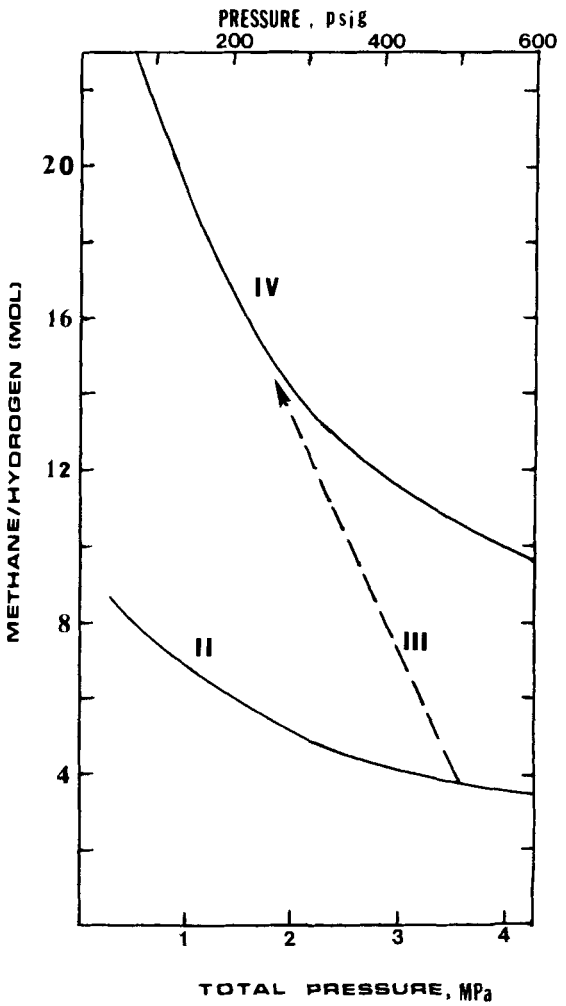

Figure 6. Total loading analysis. Ratio of total (adsorbed and gas-phase) amounts in activated carbon with 0.78 voids at 300 K, at gas-phase ratio of CH_4/H_2 = 1 (II) and 3 (IV). - - - - shift performed by Step III (200, 400, 600 psig = 1.378, 2.756, 4.134 MPa, respectively.)

15475905, 1985, 11, Downloaded from https://aiche.onlinelibrary.wiley.com/doi/10.1002/aic.690311109 by Georgia Institute Of Technology, Wiley Online Library on [06/11/2022]. See the Terms and Conditions (https://onlinelibrary.wiley.com/terms-and-conditions) on Wiley Online Library for rules of use; OA articles are governed by the applicable Creative Commons License

TABLE 5. STEADY-STATE PSA SEPARATION OF 50/50 H_2/CH_4 MIXTURE AT VARIOUS FLOWRATE (PRESSURE HISTORIES SHOWN IN FIG. 7; HIGH P = 300 psig = 2.067 MPa)

Run:	Experimental I	Experimental J	Experimental K	Theoretical I	Theoretical J	Theoretical K
Avg. Prod. in II, L/min	1.61	4.7	7.1	1.61	4.7	7.1
P/F Ratio	0.11	0.11	0.056	0.11	0.11	0.056
End Press. in III, psig	70	125	180	70	125	180
Step II Avg. H_2 %	98.4	98.4	93.5	97.6	98.6	96.5
Step II Total Amt.*	4.8	13.9	21.4	4.6	8.2	19.0
Step III Avg. H_2 %	91.9	90.3	51.9	91.3	94.0	67.1
Step III Total Amt.	10.7	7.8	6.13	10.8	7.6	5.9
Steps IV, V Avg. CH_4 %	94.8	83.2	80.2	88.4	84.9	83.2
Steps IV, V Total Amt.	15.1	26.3	27.6	16.6	22.7	28.7
Total Feed/Cycle	30.1	46.4	54.0	31.2	43.9	52.5
% H_2 Recovery	94.6	83.3	80.0	89.0	87.5	81.5
% CH_4 Recovery	93.8	94.4	83.6	94.1	87.7	90.0

* All amounts in L STP.

The role played by step III can be understood from Figure 6. The ratio of CH_4/H_2 in the zone covered by the wavefront lies on curve II in Figure 6. Without step III, going directly to steps IV and V, curve II sets the limit of the CH_4 product purity. For example, at 500 psig (3.445 MPa), the highest possible CH_4 product concentration will be 80%. With step III, the total pressure is decreased and the gas-phase concentration of CH_4 in the zone covered by the concentration wavefront is increased, e.g., to near 75% (see Figure 3), due to desorption. The ratio of CH_4/H_2 in the bed covered by the wavefront lies on a much higher position, e.g., on curve IV. The difference between curves II and IV is due to the amount of H_2 eluted from the wavefront (and subsequently out of the bed). This is possible because the bed not utilized in step II is used to adsorb CH_4 (and much less H_2) during step III. Therefore, it is seen that the role of step III is to shift the loading ratio from curve II to curve IV. For the above example where 500 psig (3.445 MPa) is cocurrently depressurized to 250 psig (1.723 MPa), the CH_4 product concentration can reach 94% during steps IV and V, as shown in Figure 6.

From Figure 6, the effects of the pressure in step II and the end pressure in step III can also be understood and predicted. It is seen that lower pressures are more favorable for separation. However, a lower pressure will result in a lower throughput, or productivity. Thus, optimal pressures must be used.

Effects of Feed Rate and Pressure

As mentioned, the feed rate was calculated from the product flowrate in step II, and was measured at the ambient pressure. Since the CH_4 concentration was very low in step II, the feed rate was approximately double the product flowrate. In Tables 5 and 6, the results of different product flowrates are given for the same time length of feed. The total feed per cycle, also given, was the sum of the feed in step II and that used in step I. This sum was taken as the sum of all effluents in steps II through V, at steady state.

The effects of feed rate should be more rationally analyzed in terms of the fraction of bed covered by the wavefront in step II. The main result of a higher feed rate, i.e., longer bed coverage in II, was a lower CH_4 product concentration, as shown by run J when compared to run I. At still higher feed rates, as in run K, the H_2 product concentration was also lowered. The concentration histories of these three runs are shown in Figures 7 and 8. The wavefront in run K, as shown in Figure 7, was apparently diffuse.

The above results can also be understood from the total loading analysis shown in Figure 6. When a large fraction of the bed is covered by the concentration wavefront in step II, a small fraction is available for cocurrent depressurization. Consequently little CH_4 is desorbed, and the CH_4 concentration in the gas phase is not increased much above 50%. The total loading of CH_4 is thus

TABLE 6. STEADY-STATE PSA SEPARATION OF 50/50 H_2/CH_4 MIXTURE AT VARIOUS FLOWRATE (PRESSURE HISTORIES SHOWN IN FIG. 8; HIGH P = 100 psig = 0.69 MPa)

Run:	Experimental L	Experimental M	Experimental N	Theoretical L	Theoretical M	Theoretical N
Avg. Prod. in II, L/min	1.6	2.8	3.6	1.6	2.8	3.6
P/F Ratio	0.19	0.13	0.11	0.19	0.13	0.11
Step II Avg. H_2 %	97.8	96.4	92.6	97.1	96.2	95.5
Step II Total Amt.*	4.4	8.3	10.7	4.4	7.7	10.0
Step III Avg. H_2 %	91.1	86.6	71.0	88.4	84.7	72.2
Step III Total Amt.	4.0	3.9	3.6	3.9	4.0	4.3
Steps IV, V Avg. CH_4 %	85.1	88.7	91.1	84.6	88.5	90.3
Steps IV, V Total Amt.	8.71	11.2	12.7	8.8	11.0	11.4
Total Feed/Cycle	16.4	22.3	25.7	16.4	21.8	25.0
% H_2 Recovery	84.7	89.0	90.1	84.2	89.2	92.2
% CH_4 Recovery	94.1	92.4	86.6	90.2	89.6	82.5

* All amounts in L STP.

15475905, 1985, 11, Downloaded from https://aiche.onlinelibrary.wiley.com/doi/10.1002/aic.690311109 by Georgia Institute Of Technology, Wiley Online Library on [06/11/2022]. See the Terms and Conditions (https://onlinelibrary.wiley.com/terms-and-conditions) on Wiley Online Library for rules of use; OA articles are governed by the applicable Creative Commons License

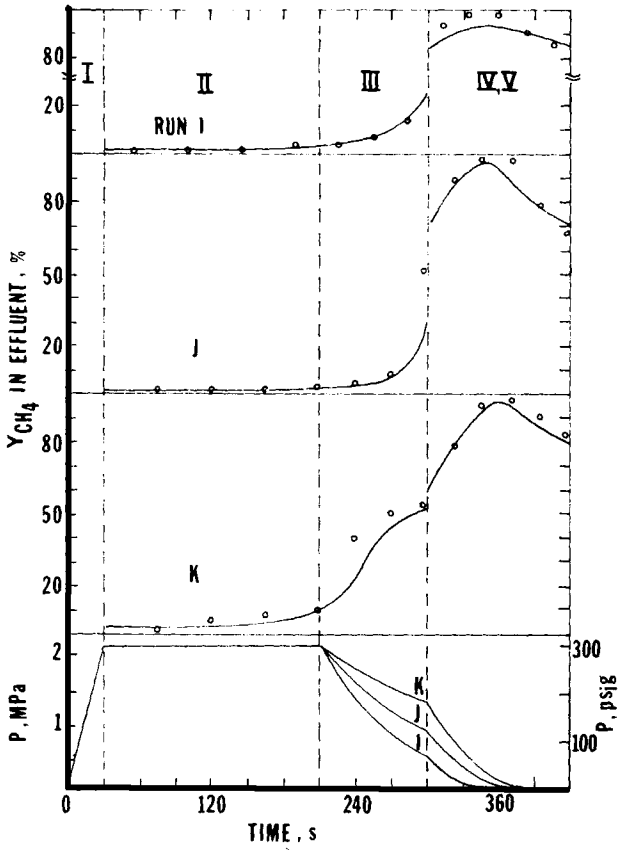

Figure 7. Effluent concentration and pressure input histories in steady-state PSA; see Table 5 for conditions. O experimental; —— predicted.

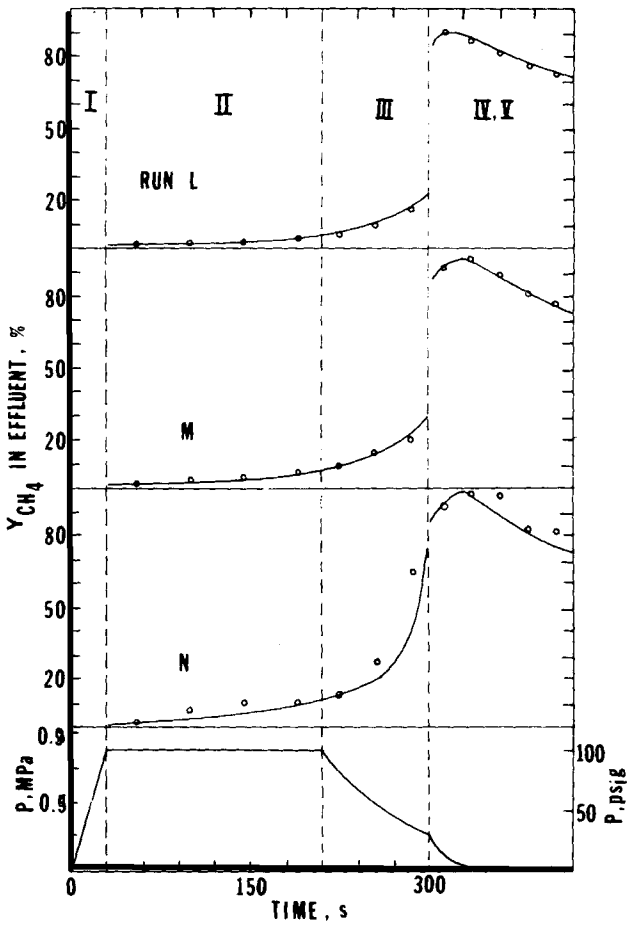

Figure 8. Effluent concentration and pressure input histories in steady-state PSA; see Table 6 for conditions. O experimental. —— predicted.

not increased much above curve II in Figure 6. [The final point(s) reached on curve IV in Figure 6 determines the CH_4 product concentration in steps IV and V.] This point was well demonstrated by the results shown in Table 5 where CH_4 concentration dropped as a higher fraction of bed was covered in step II. The bed coverage by the wavefront in step II was high in all runs shown in Table 5. The results of three runs, L, M and N, with low bed coverages by the wavefront in step II are shown in Table 6, where a low pressure was used in step II. In this case, the purge step had a significant diluting effect on the CH_4 product purity since the amount of CH_4 adsorbed in step II was small. Thus, a *higher bed coverage* yielded a higher CH_4 product purity, as shown in Table 6. If no purge was used, the CH_4 concentration would have been higher in the run with a lower bed coverage (as in run L). However, purge is beneficial for reasons described in the foregoing.

All important characteristics of PSA have been successfully predicted by the model, as shown in Tables 5 and 6, and Figures 7 and 8.

Effect of Bed Repressurization by H_2 vs. by Feed

The bed repressurization step (I) in all experiments (runs A–N) described in the preceding were performed by the feed mixture. This was in contrast to the commercial PSA processes for purification, e.g., H_2 purification. A fifteenth run (O) was made under conditions similar to run M to determine the effects of using H_2 in step I. The results of these two runs are compared in Table 7. The H_2 was introduced from the end opposite to the feed in run O, i.e., countercurrent repressurization as done in industry.

The main function of using H_2 in pressurization is to sharpen the concentration wavefront in the bed. As shown in Figure 3, the wavefront was a diffuse one after step I when the feed mixture was used. This was directly responsible for the diffuse wavefront during step II. The data shown in Table 7 indicated that the wavefront was indeed sharpened in steps II and III by H_2 pressurization. Better separation for both H_2 and CH_4 products as a result of the sharpened wavefront were also shown. The operating conditions for both runs were designed for the best results in run M. The findings for run O could have been better by changing the conditions, e.g., cocurrent blowdown to a end pressure higher than 30 psig (0.2067 MPa).

The disadvantage of using H_2 in step I is that the process is more complicated (as H_2 is obtained from the H_2 products in the process) and the throughput is somewhat lowered since a portion of H_2 is being recycled in the process.

Bed Temperatures—Adiabatic vs. Isothermal PSA

The large temperature variation in the bed is a major difference between bulk separation and purification processes. In this study, the temperature variation in the bed at any given point was generally 20–40°C. The midpoint temperature cycled by 45°C in some runs.

The temperature histories at three points for run G are shown in Figure 9 and are compared with the model predictions in the same figure. The comparison was not quantitatively good, but was satisfactory in terms of the trend of variation. The tempera-

15475905, 1985, 11, Downloaded from https://aiche.onlinelibrary.wiley.com/doi/10.1002/aic.690311109 by Georgia Institute Of Technology, Wiley Online Library on [06/11/2022]. See the Terms and Conditions (https://onlinelibrary.wiley.com/terms-and-conditions) on Wiley Online Library for rules of use; OA articles are governed by the applicable Creative Commons License

TABLE 7. COMPARISON OF EXPERIMENTAL STEADY-STATE RESULTS OF PSA SEPARATION OF 50/50 H_2/CH_4 BETWEEN PRESSURIZATION WITH H_2 AND WITH FEED MIXTURE (PRESSURE HISTORY SHOWN IN FIG. 8)

		Run			
		O		M	
Step	Time s	% CH_4	F^*	% CH_4	F^*
II	25	0.16	4.47	1.2	3.0
	70	1.0	4.35	2.7	2.84
	115	3.2	4.07	4.5	2.7
	160	5.0	3.87	6.5	2.57
III	15	7.0	3.28	8.9	3.2
	45	24.0	2.2	14.1	2.6
	75	54.7	1.5	20.0	1.94
IV & V	12	91.0	10.1	91.5	11.85
	36	97.2	5.1	95.5	5.3
	60	93.0	4.03	88.8	4.2
	84	83.0	3.57	80.5	3.7
	108	79.0	3.32	75.9	3.0
II	Avg. H_2 %	97.8		96.4	
	Total Amt.**	12.57		8.33	
III	Avg. H_2 %	77.4		86.6	
	Total Amt.	3.49		3.87	
IV, V	Avg. CH_4 %	90.0		88.7	
	Total Amt.	10.45		11.22	
Total Feed/Cycle		21.0		22.3	
% H_2 Recovery		90.0		89.0	
% CH_4		89.9		92.4	

*F in L STP/min.
** All amounts are in L STP.

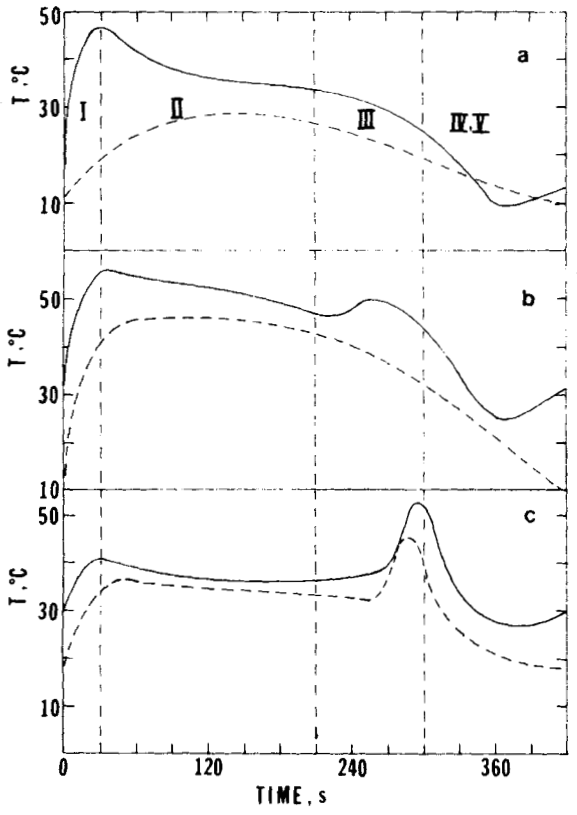

Figure 9. Steady-state PSA (Run G) temperature histograms at 12.7 cm (a); 33.0 cm (b); and 53.3 cm (c) from the top of the bed (60 cm height). —— predicted; - - - - experimental.

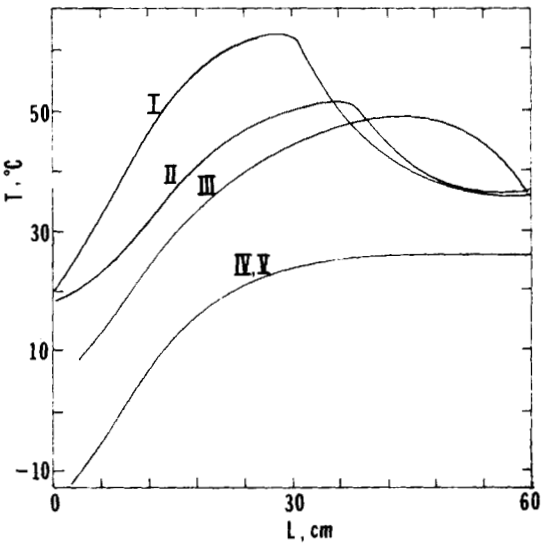

Figure 10. Predicted steady-state temperature profiles for Run G at the end of each step. *L* is distance from feed end.

ture profiles in the bed at the end of each step at steady state for run G are shown in Figure 10 from values predicted by the model.

The model has been simplified to predict a PSA process operated under isothermal conditions. The predicted isothermal results are shown in Table 8 and compared with the predicted adiabatic results for run G. Isothermal operation should give better separation than adiabatic operation for both H_2 and CH_4 products because both adsorption and desorption are improved. The comparison shown in Table 8 was not a fair one because the conditions were designed to yield the best results for run G—a higher end pressure for cocurrent blowdown in the isothermal case should have yielded a higher CH_4 product purity. Nonetheless, the comparison did show better H_2 products and a higher productivity for the isothermal case.

Effects of Pore Diffusivity and Other Sorbents

The effective pore diffusivity used in the model throughout this work was 2×10^{-4} cm^2/s as calculated for diffusion in the transition regime. An equilibrium model, by basically equating $\bar{y}$ to y, has also been formulated and compared with the experimental results (Doong and Yang, 1985). The results of the pore diffusion model are similar to those of the equilibrium model. It is

TABLE 8. COMPARISON OF THEORETICAL STEADY-STATE PSA SEPARATION OF 50/50 H_2/CH_4 BETWEEN ADIABATIC AND ISOTHERMAL OPERATIONS (PRESSURE HISTORY AS FOR RUN G FIG. 5)

	Adiabatic	Isothermal
End Press in III, psig	170	170
P/F Ratio	0.09	0.09
Step II Avg. H_2 %	98.8	99.34
Step II Total Amt.	7.93	8.25
Step III Avg. H_2 %	95.6	97.73
Step III Total Amt.	13.6	15.52
Steps IV, V Avg. CH_4 %	84.5	81.4
Steps IV, V Total Amt.	26.8	29.9
Total Feed/Cycle	47.7	53.0
% H_2 Recovery	84.2	85.3
% CH_4 Recovery	94.9	91.9

15475905, 1985, 11, Downloaded from https://aiche.onlinelibrary.wiley.com/doi/10.1002/aic.690311109 by Georgia Institute Of Technology, Wiley Online Library on [06/11/2022]. See the Terms and Conditions (https://onlinelibrary.wiley.com/terms-and-conditions) on Wiley Online Library for rules of use; OA articles are governed by the applicable Creative Commons License

clear that pore diffusion is not important under the conditions in our experiments, due to the small particle size, slow flowrates, etc. A sensitivity test was completed to compute the PSA results using the pore-diffusion model with various values of D_e. Essentially, the same results were obtained for D_e values higher than 2×10^{-4} cm^2/s. However, as D_e was lowered to 10^{-5} cm^2/s, substantially worse separation was obtained (Doong and Yang, 1985). For example, under conditions in run A, the average H_2 product purity was ($D_e = 2 \times 10^{-4}$ cm^2/s): 99.3% from step II and 93.5% from step III; whereas for $D_e = 10^{-5}$ cm^2/s: 92.4% from step II and 77.5% from step III. Thus, as predicted by the pore diffusion model, $D_e = 10^{-4}$ cm^2/s appears to be a threshold for PSA separation under run A conditions.

The D_e values in molecular sieves are generally orders-of-magnitude lower than in activated carbon. For example, the D_e values for CH_4, N_2, and most other nonpolar gases in zeolites with 4–5 Å (0.4–0.5 nm) pores are in the range of 10^{-12} to 10^{-14} cm^2/s at 20–200°C. On the other hand, the adsorption capacity in zeolites is substantially lower than in carbon. Nonetheless, it is believed that pore diffusion is very important in PSA processes using zeolites as sorbents.

CONCLUDING REMARKS

Experimental results have shown that PSA can be used for bulk separation. In this study, a 50/50 H_2/CH_4 mixture was separated into two high-purity products at a high throughput. A pore-diffusion model was formulated which successfully predicted all process characteristics.

The purge step (by H_2) is crucially important for high H_2 product purity. Repressurization of the bed by H_2, rather than by the feed mixture, is also important for high H_2 product purity.

The CH_4 product purity depends critically on the use of a cocurrent depressurization step. The main function of this step is to elute the less strongly adsorbed H_2 out of the concentration wavefront, thus increasing CH_4 loading in the bed.

The process can be optimized for specific purposes by using the model. The computation required for the model is not excessive. That is, approximately 1 min/cycle is required on a Cyber 730 computer, and 10 cycles are adequate to reach cyclic steady state from startup for the specific separation system considered in this study.

ACKNOWLEDGMENT

This work was supported by the U.S. Department of Energy under Grant No. DE-AC21-83MC20183.

NOTATION

a = average radius of sorbent particle, cm; or constant in Eqs. 15 and 16
A = cross-sectional area, cm^2
b = constant in Eqs. 15 and 16
B = a constant related to the net ethalphy, ΔH, of adsorption according to Langmuir theory, MPa^{-1}
C = concentration of sorbate in bulk flow, mol/L
C_P = heat capacity, cal/mol/K
D_e = effective diffusivity of sorbate, cm^2/min or cm^{2}s
$D_{k,m,t}$ = diffusivity in Knudsen, molecular, and transition regimes, respectively
F = flow rate of effluent, L STP/min
h = heat transfer coefficient between bed and wall, cal/cm^2/K/s
n = constant in Eq. 28
N = molar flux, mol/cm^{2}s
P = total or partial pressure, MPa or psi
q = number of moles of sorbate adsorbed per gram of solid, mol/g of solid
Q = heat of adsorption, cal/mol
r = radial distance from center of spherical particle, cm
R = gas constant
S = overall rate of sorption per unit volume of bed, mol/L/min
t = time, min or s
T = solid or bed temperature, K
u = superficial velocity, cm/min or cm/s
y_i = mole fraction of species i
z = axial distance along the bed in feed direction, cm

Greek Letters

α = interparticle void fraction
Δt = time step, min
ϵ = intraparticle void fraction
ρ_B = bed density, g/cm^3
ρ_P = particle density, g/cm^3
τ = tortuosity

Subscripts

A = CH_4
B = H_2
b = bed
i = species, or cell or shell number
p = particle
m = monolayer coverage
w = wall of the column

Superscripts

s = surface of particle
$\bar{}$ = volume-average quantity

LITERATURE CITED

Aris, R., "Equilibrium Theory of Parametric Pump," *Ind. Eng. Chem. Fund.*, **8**, 603 (1969).

Carter, J. W., and M. L. Wyszynski, "The Pressure Swing Adsorption Drying of Compressed Air," *Chem. Eng. Sci.*, **38**, 1,093 (1983).

Cassidy, R. T., and E. S. Holmes, "Twenty-Five Years of Progress in Adiabatic Adsorption Processes," *AIChE Symp. Ser.*, **80**(233), 68 (1984).

Chan, Y. N., F. B. Hill, and Y. H. Wong, "Equilibrium Theory of a Pressure Swing Adsorption Process," *Chem. Eng. Sci.*, **36**, 243 (1981).

Chen, W. N., and R. T. Yang, "Adsorption of Gas Mixtures and Modeling Cyclic Processes for Bulk, Multicomponent Gas Separation," *Recent Developments in Separation Science*, N. N. Li and J. M. Calo, Eds., CRC Press, Cleveland, **IX** (1985).

Cheng, H. C., and F. B. Hill, "Recovery and Purification of Light Gases by Pressure Swing Adsorption," *Industrial Gas Separations, ACS Symp. Ser.*, **223**, 195 (1983).

Chihara, K., and M. Suzuki, "Simulation of Nonisothermal Pressure Swing Adsorption," *J. Chem. Eng. Japan*, **16**, 53 (1983a).

———, "Air Drying by Pressure Swing Adsorption," *J. Chem. Eng. Japan*, **16**, 293 (1983b).

Doong, S. J., and R. T. Yang, "When Is Pore Diffusion Important in Pressure Swing Adsorption for Gas Separation?" *Chem. Eng. Commun.*, (1985).

Fernandez, G. F., and C. N. Kenney, "Modeling of the Pressure Swing Air Separation Process," *Chem. Eng. Sci.*, **38**, 827 (1983).

15475905, 1985, 11, Downloaded from https://aiche.onlinelibrary.wiley.com/doi/10.1002/aic.690311109 by Georgia Institute Of Technology, Wiley Online Library on [06/11/2022]. See the Terms and Conditions (https://onlinelibrary.wiley.com/terms-and-conditions) on Wiley Online Library for rules of use; OA articles are governed by the applicable Creative Commons License

Hill, F. B., Y. W. Wong, and Y. N. I. Chan, "A Temperature Swing Process for Hydrogen Isotope Separation," *AIChE J.*, **28,** 1 (1982).
Jenczewski, T. J., and A. L. Myers, "Parametric Pumping Separates Gas Phase Mixtures," *AIChE J.*, **14,** 509 (1968).
Jones, R. L., and G. E. Keller, "Pressure-Swing Parametric Pumping—A New Adsorption Process," *J. Separ. Proc. Technol.*, **2**(3), 17 (1981).
Keller, G. E., "Gas-Adsorption Processes: State of the Art," *Industrial Gas Separations*, T. E. Whyte, Jr., et al., Eds., Am Chem. Soc., Washington, DC, 145 (1983).
Kowler, D. E., and R. H. Kadlec, "The Optimal Control of a Periodic Adsorber," *AIChE J.*, **18,** 1,207 (1972).
Liaw, C. H., J. S. P. Wang, R. A. Greenkorn, and K. C. Chao, "Kinetics of Fixed-Bed Adsorption: A New Solution," *AIChE J.*, **25,** 376 (1979).
Nataraj, S., and P. C. Wankat, "Multicomponent Pressure Swing Adsorption," *Recent Advances in Adsorption and Ion Exchange*, Y. H. Ma, et al., Eds., *AIChE*, New York, **78** (1982).
Pigford, R. L., B. Baker, and D. E. Blum, "An Equilibrium Theory of the Parametric Pump," *Ind. Eng. Chem. Fund.*, **8,** 144 (1969).
Saunders, J. T., "Adsorption of H_2 and CH_4 from Single and Mixed Gases," M.S. Thesis, Department of Chemical Engineering, SUNY at Buffalo, Amherst, NY (1982).
Shendalman, L. H., and J. E. Mitchell, "A Study of Heatless Adsorption in the Model System CO_2 in He," *Chem. Eng. Sci.*, **27,** 1,449 (1972).
Skarstrom, C. W., "Use of Adsorption Phenomenon in Automatic Plant-Type Gas Analyzers," *Ann. NY Acad. Sci.*, **72,** 751 (1959).
Stewart, H. A., and J. L. Heck, "Pressure Swing Adsorption," *Chem. Eng. Prog.*, **65,** 78 (1969).
Sweed, N. H., and R. H. Wilhelm, "Parametric Pumping," *Ind. Eng. Chem. Fund.*, **8,** 221 (1969).
Tsai, M. C., S. S. Wang, and R. T. Yang, "Pore Diffusion Model for Cyclic Separation," *AIChE J.*, **29,** 966 (1983).
Turnock, P. H., and R. H. Kadlec, "Separation of Nitrogen and Methane via Periodic Adsorption," *AIChE J.*, **17,** 335 (1971).
Wankat, P. C., "Cyclic Separation Techniques," *Percolation Processes, Theory and Application*, A. E. Rodrigues and D. Tondeur, Eds., Alphen Ann Den Ryn, Netherlands, 443 (1981).
Weaver, K., and C. E. Hamrin, Jr., "Separation of Hydrogen Isotopes by Heatless Adsorption," *Chem. Eng. Sci.*, **29,** 1,873 (1974).
Yagi, S., and N. Wakao, "Heat and Mass Transfer from Wall to Fluid in Pack Beds," *AIChE J.*, **5,** 79 (1959).
Yang, R. T., and R. T. Liu, "Gaseous Diffusion in Porous Solids at Elevated Temperatures," *Ind. Eng. Chem. Fund.*, **21,** 262 (1982).
Yon, C. M., and P. H. Turnock, "Multicomponent Adsorption Equilibria on Molecular Sieves," *AIChE Symp. Ser.*, **67**(117), 3 (1971).

Manuscript received Apr. 24, 1984; revision received Nov. 2, 1984 and accepted Jan. 8, 1985.

15475905, 1985, 11, Downloaded from https://aiche.onlinelibrary.wiley.com/doi/10.1002/aic.690311109 by Georgia Institute Of Technology, Wiley Online Library on [06/11/2022]. See the Terms and Conditions (https://onlinelibrary.wiley.com/terms-and-conditions) on Wiley Online Library for rules of use; OA articles are governed by the applicable Creative Commons License